The Unequal Socioeconomic Risks of Global Terrestrial Moisture Recycling

Sandy Sum[1], Simon Fahrländer[2], Lauren S. Andersen[2], Richard Damania[3], Johan Rockström[2], Ram Fishman*[4], and Tamma Carleton*[5]

[1]University of California, Davis
[2]Potsdam Institute for Climate Impact Research (PIK)
[3]World Bank
[4]Tel Aviv University
[5]University of California, Berkeley and National Bureau of Economic Research

January 9, 2026

Abstract

The global hydrological cycle depends on an atmospheric transport network in which water evaporating from one location ultimately falls as precipitation in another. Within this network, linkages between land sources and land sinks, collectively referred to as terrestrial moisture recycling (TMR), occupy a prominent role. Changes in land use, such as deforestation, can disrupt this water transport network, threatening both economic stability and food security. Here, we quantify these socioeconomic risks on a global scale by integrating high-resolution bilateral atmospheric flow models with geospatial socioeconomic data and econometric analysis. We find that the risks from TMR disruption are highly unequal: low-income populations reliant on rainfed agriculture are disproportionately dependent on TMR for precipitation, while the world's wealthiest regions benefit from abundant, relatively stable ocean-based precipitation. We estimate that TMR disruption from forest loss in emerging deforestation hotspots could have large and unequal socioeconomic implications, causing a 0.11 percentage point (*p.p.*) drop in the average global GDP growth rate, with particularly strong impacts in Africa (0.24 *p.p.*) and South America (0.36 *p.p.*). These emerging deforestation threats could fully reverse growth in agricultural productivity across Africa and cause widespread agricultural losses in South America and Asia. In contrast, Australia, Europe, and North America are insulated from deforestation-based TMR disruption. These findings highlight previously under-appreciated elements of the economic value provided by forests. They provide the first blueprint for global economic governance of land-based moisture flows and can help target land conservation priorities to maximize moisture recycling benefits.

*Correspondence to: tcarleton@berkeley.edu, ramf@tauex.tau.ac.il. These authors jointly supervised this work.
We thank Maren Ludwig for excellent research assistance. Funding was generously provided by the Global Commission on the Economics of Water.

Introduction

Terrestrial moisture recycling (TMR) – the process of moisture evaporating from the Earth's surface, traveling atmospherically, and later falling as rain – plays a key role in shaping global precipitation patterns[1–4]. Increasingly detailed characterizations of TMR in high-resolution moisture tracking models suggest that significant portions of precipitation falling on land originate from terrestrial evapotranspiration (ET). On average, 45% of all terrestrial rainfall globally is estimated to originate from land-based evapotranspiration[5], rather than from ocean evaporation. In turn, about 60% of global terrestrial precipitation returns to the atmosphere via evapotranspiration[6], with the remainder stored in soils as green water or as blue water in rivers, lakes, and aquifers. Given this interdependence, human-induced changes to land use – such as deforestation, forestation, and crop irrigation – can alter these patterns of TMR, affecting downwind rainfall patterns[7–9] and rainfall-dependent economic outcomes, such as agricultural yields and hydropower generation[10–14].

These new insights are beginning to spur nascent efforts advocating for land and water co-governance[1,15–17]. Yet the translation of TMR research into globally-comprehensive, comparable, and communicable economic metrics for policymaking remains limited. Existing studies remain geographically restricted[16,18] and generally focus on specific examples of forest-based interventions[11,13]. As a result, TMR is largely left out in land management and water policy discussions[1,3]. No existing assessments comprehensively diagnose global water scarcity risks from TMR, accounting for both the potential hazard posed by land use change in the source location(s) and for the socioeconomic exposure and vulnerability of the sink location. In the absence of a structured risk diagnosis, consistent with those used in climate assessments such as the IPCC's[19], opportunities to identify where targeted interventions could mitigate the risks of terrestrial moisture flow disruption to water and food security remain unrealized[17].

Here, we combine a high-resolution global model of atmospheric moisture flows with granular socioeconomic and land use data as well as econometric analysis of economic dependence on rainfall to conduct a global socioeconomic risk assessment of TMR and its potential disruption. First, we identify which populations and global regions are most socioeconomically dependent on TMR. We then determine the land types and regions of the globe that generate the moisture flows these populations depend on, revealing a substantial role for both forests and agricultural lands in generating present-day moisture recycling. Finally, we quantify the economic implications of TMR disruption from deforestation threats and how this burden is distributed unequally across the globe. Our results reveal regions and populations most socioeconomically dependent on a stable atmospheric water cycle, while also uncovering the source regions responsible for generating the most economically valuable evapotranspiration. These insights can help conservation policies target "hotspots" in which changes to land use, such as irrigation and deforestation, are likely to have significant downwind social and economic consequences via TMR. They can similarly help target policies to protect populations and ecosystems in locations that are highly vulnerable to TMR disruptions.

To implement our analysis, we leverage cell-to-cell atmospheric moisture flows at 1° spatial resolution derived using the UTrack model[20], a bilateral matrix of atmospheric source-to-sink flows based on Lagrangian moisture tracking[21]. These data represent a 10-year average of moisture transfers over the 2008-2017 period. In the UTrack model, evaporation is simulated as parcels of moisture that are tracked through the atmosphere, accounting for wind-driven transport and probabilistic vertical movement, similar to how air pollution is tracked in models such as HYSPLIT[22]. The model and dataset are widely used in recent investigations of TMR[15,23–26]. Complementary approaches based on satellite observations and water vapor isotopes have also been used to trace precipitation sources, providing independent evidence for moisture recycling pathways and hydroclimatic vulnerabilities[27,28].

We integrate a rich compilation of geospatial data with UTrack outputs to assess exposure to TMR-based risks (Fig. 1). For each terrestrial 1° cell, we quantify the land use characteristics of its precipitation "source" regions – the upwind land surface contributing to local precipitation – to uncover how forests, croplands, and other land cover types heterogeneously generate recycled moisture across diverse global regions. Similarly, we investigate the socioeconomic vulnerability of each cell's ET "sink" regions – the downwind locations where ET generated in a given source cell lands as precipitation – to reveal locations generating moisture destined for sustaining livelihoods downwind. Each grid cell globally serves as both a sink (Fig. 1a, c) and a source (Fig. 1b, d), allowing us to assess both the places most dependent on TMR as well as those responsible for generating the most economically valuable moisture flows. For example, much of the terrestrial-sourced precipitation landing in Mato Grosso, Brazil originates in the densely forested Amazon (Fig. 1a), while terrestrial precipitation flowing into WaKeeney, Kansas originates almost exclusively from non-forested areas (Fig. 1c). Additionally, evaporation from WaKeeney largely recycles back into local rainfed croplands (Fig. 1d), whereas only a small share of evaporation from Mato Grosso, Brazil (Fig. 1b) reaches downwind crops. These contrasting cases illustrate the large heterogeneity in both the economic value of each source and the economic vulnerability of each sink globally.

For each terrestrial locality, vulnerability to TMR disruption depends on (i) upwind land use patterns and their contributions to precipitation, (ii) exposure of the local population and agriculture to precipitation derived from TMR, and (iii) the vulnerability of local social and economic systems to variations in rainfall. In the following analysis, we integrate atmospheric flows, land cover, economic, and human settlement data to systematically assess the global distribution of socioeconomic risks posed by TMR disruption. We then simulate the economic and agricultural impacts of deforestation by combining modeled losses in TMR, driven by deforestation in key hotspots, with econometric analysis that captures the non-linear relationship between precipitation and economic productivity.

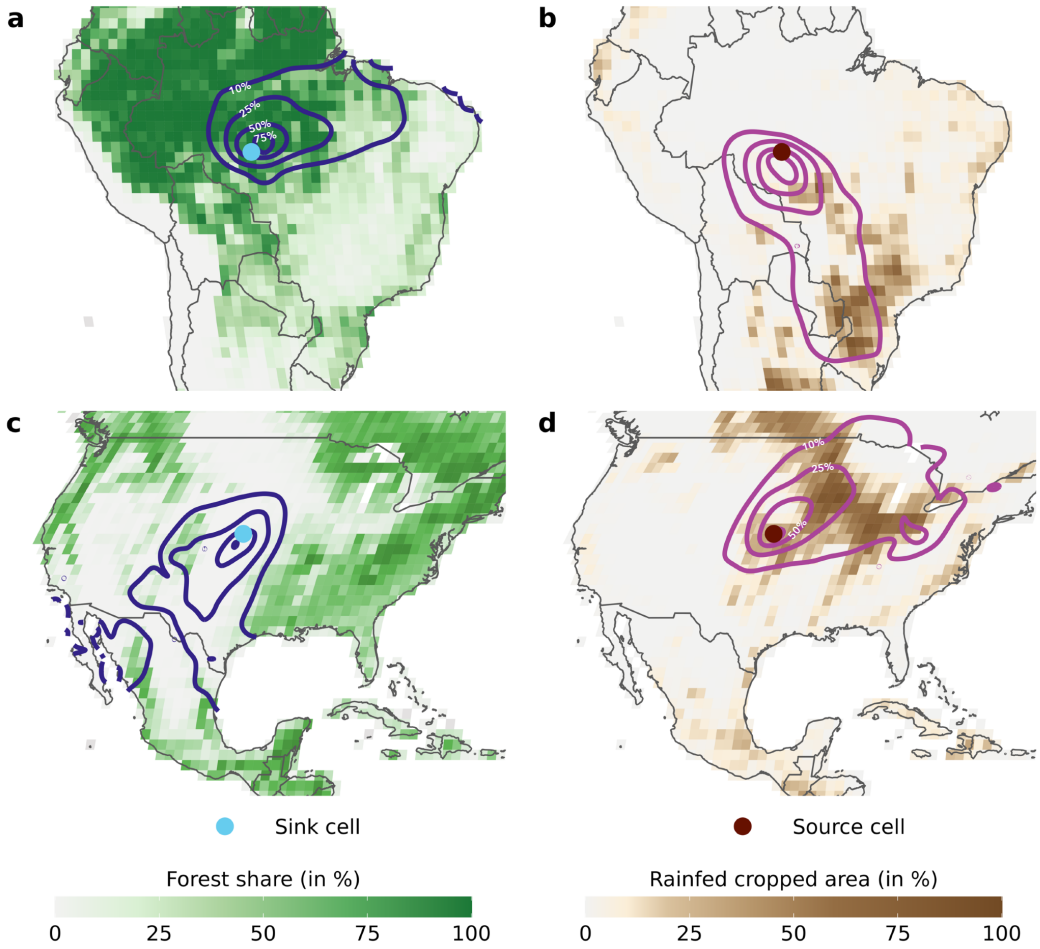


Figure 1: Diversity of land use and socioeconomic vulnerability across global terrestrial moisture dependencies. Figure panels show contour lines delineating the source and destination of moisture for two example grid cells: Mato Grosso, Brazil (**a, b**) and WaKeeney, Kansas, U.S. (**c, d**). The blue nodes in **a** and **c** indicate example sink locations, with contour lines indicating the spatial distribution of upwind moisture sources by quantity of rainfall contributed. Cells along each contour line contribute the same amount of rainfall to the sink cell. The underlying heat map in green plots the share of forest cover in each cell. Panels **b, d** show these two locations as source locations, plotting the destinations of local evapotranspiration for the same two locations by quantity of rainfall. Cells along each contour line in **b** and **d** receive the same amount of rainfall from the source cell. The underlying heat maps in brown plot the share of rainfed cropped area in each cell. Contour lines delineate points contributing (receiving) 10%, 25%, 50%, and 75% of the maximum observed terrestrial precipitation (evapotranspiration) contributed or received by a cell, respectively.

Results

Low-income regions and rainfed croplands are disproportionately dependent on terrestrial moisture recycling

We assess the vulnerability of each 1° grid cell location across the globe to potential disruptions in TMR. For each location, we calculate the *terrestrial precipitation share*: i.e., the component of precipitation originating from terrestrial sources of moisture – as opposed to oceanic sources – expressed as a percentage of total precipitation. This metric reveals regions where precipitation may be significantly affected by TMR disruptions resulting from upwind land use change.

In line with previous work[4,20], we uncover substantial global heterogeneity in the terrestrial precipitation share, indicating widely varying degrees of dependence on land-based TMR (Fig. 2a). There are many geographic hotspots with high reliance on TMR, including much of Central Africa, lower South Africa, and the Tibetan Plateau, where the terrestrial precipitation share exceeds 75%. In contrast, in the Western US, Western Europe, Eastern Brazil, and much of Southeast Asia, the vast majority of rainfall originates from the oceans, a stable source of moisture. We estimate that just above 18% of all global grid cells have *high dependence* on TMR, defined as those receiving over 75% of precipitation from TMR.

TMR-dependent regions are disproportionately low-income (Fig. 2b): among high-dependency grid cells, 33% are characterized as low-income (<4,465$ annual income, following World Bank classifications), whereas low-income locations only make up 14% of grid cells globally. 40% of grid cells in the lowest global income decile have high TMR dependency, compared to just 2.4% in the richest decile. Moreover, distributions of terrestrial precipitation share are highly skewed in lower income regions, such that a few localities are highly vulnerable: 20% of the grid cell areas in lowest income decile – significantly dominated by Central Asia, Western China, and Central Africa – receive 95% or more of their rainfall from terrestrial sources.

Integrating local income data reveals the regressive nature of TMR-related risks. However, the *magnitude* of the impact on these groups will depend on the size of the local population – which depends on freshwater to meet basic needs – and the extent of rainfall-dependent economic activity. Rainfed agriculture is a particularly important driver of vulnerability, as agriculture is humanity's most water-intensive economic activity[30] and rainfed crop lands are entirely dependent on the local hydroclimate. We find that human populations are disproportionately concentrated *away* from regions of high TMR dependence: just 14% of the globe's population is settled in areas with terrestrial precipitation share exceeding 75% (Fig. 2d). However, in some locations, TMR dependence coincides strongly with rainfed cropping systems, such that agricultural productivity in those locations is heavily exposed to impacts from upwind land use change (Fig. 2c). These high-exposure areas extend across Sub-Saharan Africa, the Indo-Gangetic Plain, the US Great Plains, Eastern Europe, Southern Brazil and Northern Argentina, and Eastern China. We also identify

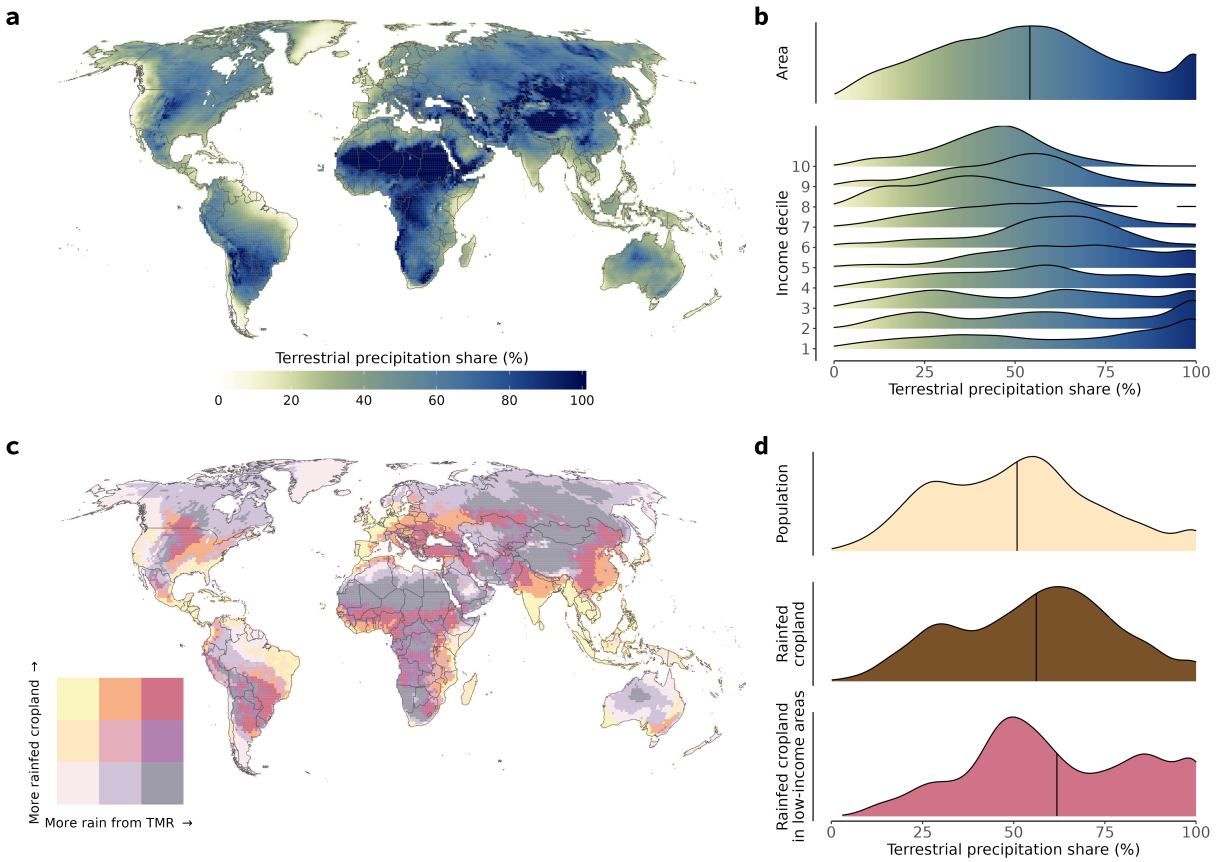


Figure 2: Global estimates of terrestrial precipitation share across space, socioeconomic conditions, and land use. Map **a** shows the share of total precipitation originating from terrestrial sources, as opposed to originating from the ocean for each terrestrial location ($N = 17,674$) on Earth. Plot **b** shows the overall (top panel) and conditional (bottom ten panels) distributions of terrestrial precipitation share for each decile of the income distribution, with category one being the lowest decile. Regions are divided into income categories using gridded GDP estimates from ref.[29]. Map **c** overlays the spatial distribution of rainfed cropland share and reliance on TMR (from **a**) using a bivariate color scheme. The horizontal axis of the legend represents the terrestrial precipitation share, while the vertical axis denotes the share of land allocated to rainfed cropland. Locations in dark pink represent high vulnerability to TMR disruption. Plot **d** displays distributions of terrestrial precipitation share weighted by population count (top panel), rainfed cropland (middle panel), and rainfed cropland only in low-income regions (GDP per capita below 4,456 USD) (bottom panel).

other regions with high TMR dependence – such as Western China and the Middle East – that devote little to no land to agriculture, likely due to other biophysical constraints such as poor soils or low fertility, that make cultivation unsuitable. Globally, we estimate that 20% of all rainfed croplands receive over 75% of their precipitation from terrestrial sources. TMR dependence is even higher in low income regions, where 37% of rainfed croplands exceed this 75% threshold (Fig. 2d, bottom).

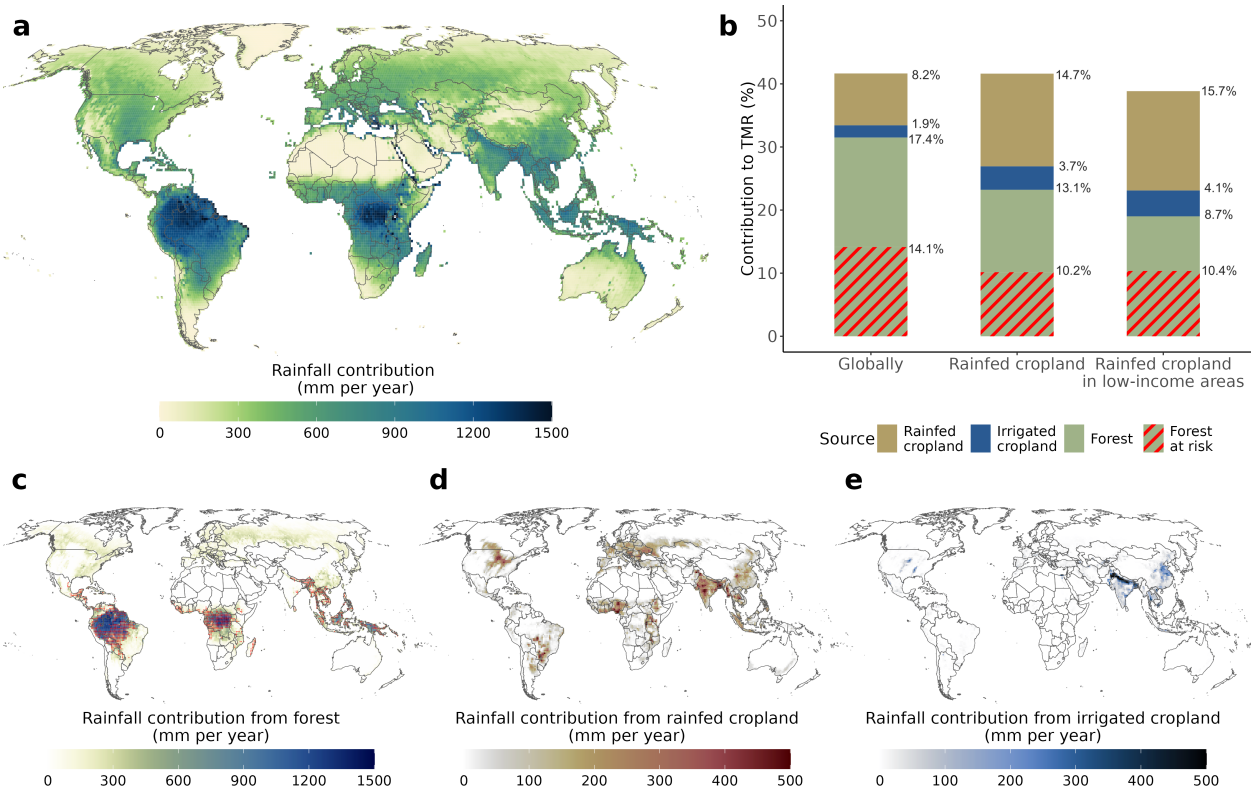


Figure 3: Sources of terrestrial precipitation globally. Map **a** shows the average annual quantity of moisture generated by evapotranspiration (ET) in each location ($N = 17,674$) over the period 2008-2017 that ultimately falls as precipitation on other terrestrial locations. Barplot **b** shows the share of total rainfall that is generated through terrestrial moisture recycling (TMR) globally (left column), in all rainfed cropland (middle column), and in rainfed cropland in low-income areas (right column), with land cover types of source regions colored in green (forest), blue (irrigated croplands), and brown (rainfed croplands). The share of TMR originating from emerging deforestation hotspots, as defined by ref.[31], is indicated by red stripes. Maps **c**, **d**, and **e** show the average annual quantity of moisture generated by evapotranspiration (ET) from forest, rainfed cropland, and irrigated cropland, respectively. In map **c** emerging deforestation hotspots are highlighted through red stippling. See Methods for a description of how moisture contributions are partitioned into their respective source and sink categories.

Forests under threat generate significant rainfall destined for vulnerable regions

From where do TMR-dependent regions derive their rain? We find, consistent with prior work[20,24,32–34], that the most important sources of TMR – locations with the highest shares of ET destined for other land areas – are the Congo River basin in Africa, the Amazon forest in South America, and the tropical rainforests of South Asia and South East Asia (Fig. 3a). In aggregate, these forested lands account for over 30% of all terrestrial-sourced precipitation (Fig. 3c, Table S1), but they are under increasing threat of land use change, primarily due to agricultural expansion[35,36]. This potential disruption raises concerns for downwind locations currently relying on forest-based ET. We

estimate that lands currently classified as deforestation "hotspots" (see Methods for details) generate geographically concentrated pockets of TMR-based risk for downwind communities (Fig. S3a). Specifically, the Republic of the Congo, Democratic Republic of the Congo, and a handful of other West Central African nations contain lands in which over 75% of annual rainfall originates from emerging deforestation hotspots where the current supply of ET is severely threatened. Similarly, a swath of land just east of the Andes in South America exhibits heavy dependence on rainfall from rapidly deforesting regions of the Amazon.

The economic risks posed by the transformation of emerging deforestation hotspots are disproportionately large for rainfed croplands in low-income regions of the globe. We find that these regions source more than 10% of their precipitation from emerging deforestation hotspots on average, a share that exceeds both the average on all rainfed croplands and the average across all global regions (7% and 4%, respectively; Fig. S3b). These findings suggest that the populations most vulnerable to precipitation changes – i.e., rainfed agricultural economies with adaptive capacities constrained by low incomes – may face the highest risk from TMR disruptions.

Crop-to-crop moisture recycling contributes to local rainfall in vulnerable regions

Non-forested lands are also found to play critical roles in TMR generation, particularly for generating rainfall in agricultural regions. These non-forested lands include former forests converted to cropland, as well as other land cover types, including grasslands; wetlands; and water bodies. Globally, we estimate that 8% of terrestrial-sourced precipitation originates from rainfed cropland, about 2% from irrigated cropland, with the rest coming from all other land cover types (Fig. 3b, Table S1). While forests historically generated higher ET, the apparent influence of cropland today in areas where forests once dominated arises both from their position within the moisture flow network and from their vegetated surface, which enables ET compared to non-vegetated or impervious land covers[37]. Rainfed agriculture in South and Southeast Brazil, the Midwest of North America, and much of Europe and South and Southeast Asia continues to make significant contributions to TMR today (Fig. 3d). Isolated areas of the Great Plains in North America, along with a wide swath of northern India and eastern China with intensive irrigated farming also emerge as critical TMR source locations (Fig. 3e), contributing to downwind rainfall.

Moisture recycling between agricultural sink and source regions is quantitatively substantial. We find that rainfed cropland receives nearly twice as much precipitation from other rainfed cropland (15%) than does a global average grid cell (8%). Cropland tends to span large contiguous areas and be clustered geographically, creating stronger linkages within the moisture flow network. Furthermore, up to 4% of terrestrial-sourced precipitation in rainfed cropland originates from irrigated cropland (as compared to just 2% in the global average grid cell) (Fig. 3b, Table S1). In contrast, rainfed croplands depend relatively less on ET from forests: forests contribute 23% of total rainfall on rainfed agricultural lands, compared to the global average of 30%. In low-income regions, this

dependence on within-agriculture flows is particularly stark, as rainfed agriculture depends more on ET from other croplands (20% of rainfall) than it does from forests (19% of rainfall). These findings highlight the under-recognized role that croplands play in sustaining precipitation in highly vulnerable rainfed-dependent regions today, despite having replaced the natural landscapes that preceded them. Recognizing this dual role can help guide policies that manage these landscapes and their conversion, for both food supply and moisture generation benefits[38,39].

Fig. S2b maps these contributions and shows that the most important source regions for moisture destined for rainfed agricultural lands are concentrated in India and Southern China, parts of Indonesia, parts of Eastern and Western Africa and parts of Southern Brazil. Northeast India and Eastern and Western Africa are particularly essential for sourcing moisture falling as precipitation on rainfed agricultural lands in low-income regions (Fig. S2c). The difference between the spatial patterns in Figs. 3a and S2b and c highlights that prioritizing the conservation of TMR flows that are most socioeconomically valuable may lead to very distinct planning decisions than conservation of ET flows in aggregate.

Estimates of the economic costs of TMR disruption

We quantify the economic impact of TMR disruption due to potential future deforestation. We focus on emerging deforestation "hotspots" covering 3.9 million km^2 (~10% of global forest area in 2024) that together represent the most urgent near-term risks to terrestrial moisture recycling globally[31]. Specifically, we simulate a scenario in which all hotspots are deforested, reducing local evapotranspiration (ET) in these regions to counterfactual levels observed to prevail under alternative land use types (e.g., grassland, pasture, or soybean agriculture) (see Economic valuation). We then trace the resulting changes in ET through our source-to-sink TMR flow matrix to estimate resulting reductions in downwind precipitation. To assess the monetized value of this TMR disruption, we estimate econometric regression models linking aggregate economic output[40,41] and agricultural productivity[42] to changes in precipitation and use these estimated models to translate simulated precipitation declines into monetized economic damages. Our econometric models capture the global-scale, nonlinear, spatially-varying impact of precipitation on economic output and we propagate their statistical uncertainty through subsequent simulations.

In every location, economic impacts depend on three factors: (i) the overall level of annual precipitation; (ii) the share of total precipitation originating from moisture evapotranspired from forests under threat; and (iii) and the category of baseline economic development, which determines economic vulnerability to declines in precipitation (see Fig. M1 for a schema). Our approach accounts for all three, as well as statistical uncertainty using a blocked bootstrap method[43]. We account for model-based uncertainty by relying on datasets and methodologies from two independent sources[40,41] with distinct data sources and scopes, time frames of analysis, and econometric specifications. To assess global agricultural production damages from TMR disruption, we estimate

the effect of precipitation on agricultural total factor productivity (TFP), replicating the analysis in ref.[42]. Agricultural TFP measures the overall efficiency at which farmers use inputs such as land, labor, and machinery to grow crops and livestock. In regions where cropland relies primarily on precipitation as a water source, variations in precipitation directly affect crop yields, which then affect TFP[44]. Details on our methodology are provided in Methods.

Gross domestic product impacts The economic impacts of TMR disruption in emerging deforestation hotspots are large and vary substantially across space due to differences in exposure to precipitation declines and vulnerability to this climatological shock (Fig. 4). Estimated growth impacts are, on average, largest across Africa and South America, continents that also have the largest share of total precipitation originating from TMR (Fig. 4b). In Africa, we estimate that disruptions to TMR in deforestation hotspots could reduce average annual rates of growth in GDP per capita by -0.09 (95% two-sided confidence interval: -0.12, -0.06) to -0.24 (-0.31, -0.17) percentage points (pp), with the range indicating model-based uncertainty from refs.[41] and[40]. In South America, growth impacts range from -0.08 p.p. (-0.12, -0.05) to -0.36 p.p. (-0.47, -0.24) across models. These magnitudes are substantial, reducing Africa's current annual average growth rate by 2-7% and South America's by 4-16%. In contrast, effects in Australia, Europe, and North America are virtually nonexistent, given minimal deforestation risk and low dependence on TMR. Fig. S4 maps the resulting grid cell-level estimates of the changes in GDP growth rates from TMR disruption in emerging deforestation hotspots, revealing that locations most strongly affected are concentrated in Central Africa and North-western South America and, to a lesser extent, in Southeast Asia. Overall, the analysis implies that the economic costs of precipitation reductions from deforestation threats are concentrated in low- and middle-income countries – with substantial impacts on regional economic growth rates.

Agricultural productivity impacts We find that ET losses from emerging deforestation hotspots, modeled to levels commonly observed in alternative land use, considerably diminishes agricultural productivity growth across nearly all regions, with these effects being more pronounced than those on GDP growth (Fig. 4a). As above, the largest burden falls on Africa, where annual growth rates in agricultural productivity fall by -0.73 p.p. (-0.95, -0.51), essentially removing gains realized in recent years across the continent, where average TFP growth today amounts to just ∼0.5% per year. In South America, baseline agricultural TFP growth rates are relatively high at over 2% per year, but deforestation hotspots supply substantial local rainfall (Fig. 4b), leading to TFP growth rate reductions of -0.57 p.p. (-0.74, -0.39) on average. In Asia, TMR disruption lowers agricultural growth rates by -0.39 p.p. (-0.51, -0.27) on average, while effects in Australia, Europe, and North America are small or even beneficial. In general, the locations of the globe where agriculture is most impacted by TMR disruption are similar to those experiencing severe aggregate GDP growth impacts (i.e., Central Africa, north-western South America, and much of Asia) (Fig. S5a). This suggests that agricultural productivity plays a critical role in driving GDP losses under dry conditions, consistent with prior work[40,45].

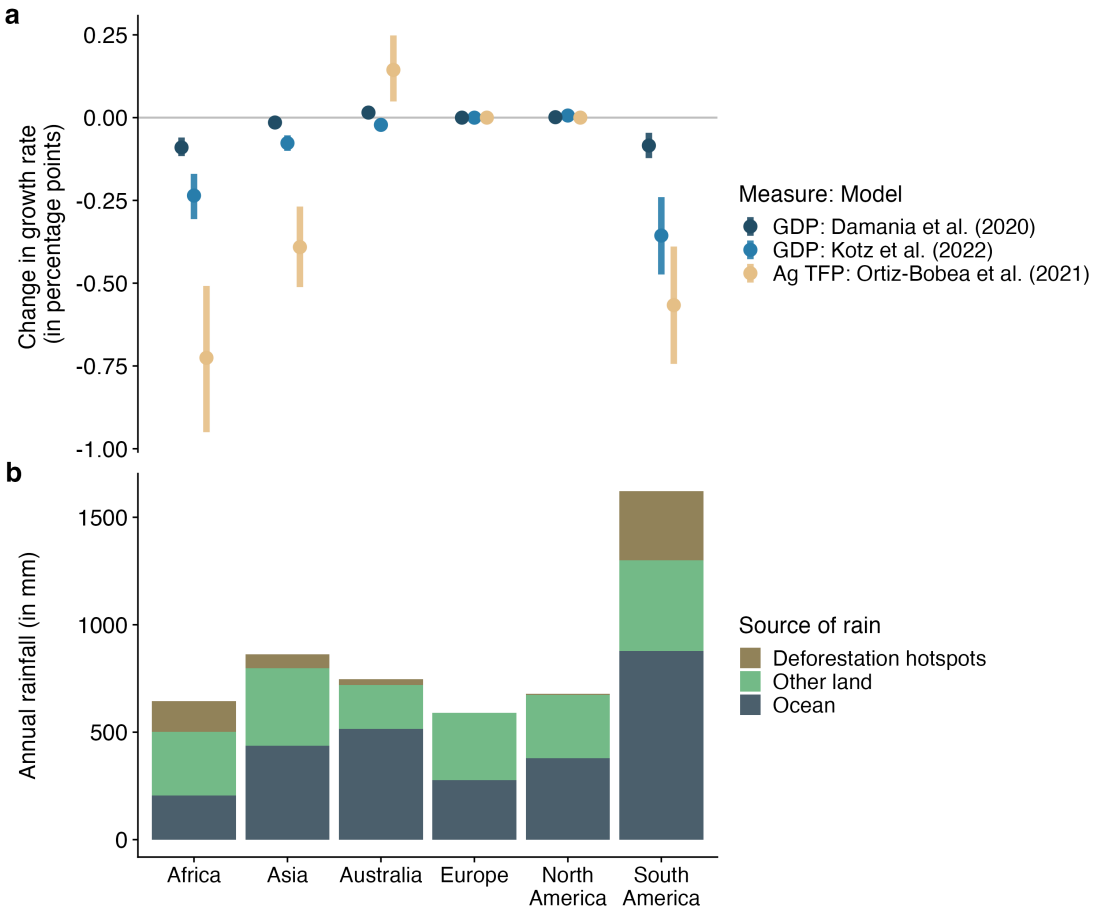


Figure 4: Impacts of removing terrestrial moisture flows from global emerging deforestation hotspots on economic and agricultural productivity growth rates. Plot **a** shows the estimated average change in the growth rate of gross domestic product (GDP; in blue) and agricultural total factor productivity (ag TFP; in beige) caused by a modeled decrease in evapotranspiration from emerging deforestation hotspots to levels observed in alternative land use. Averages are computed across all countries within each continent listed. Changes are calculated using estimates of the impact of precipitation on: *(i)* economic growth following ref.[40] in light blue; *(ii)* economic growth following ref.[41] in dark blue; and *(iii)* agricultural productivity following ref.[42]. Dots indicate the point estimates while error bars indicate statistical uncertainty in the growth rate change estimates using two-sided 95% confidence intervals obtained through block bootstrapping (see Appendix 2 for details). Plot **b** shows the breakdown of precipitation by source type: emerging deforestation hotspots (brown), other land (green), and the ocean (blue), aggregated by continent.

Discussion

Human activity is responsible for widespread changes to land use on global scales, primarily through cultivation and deforestation. A large body of research has attempted to understand and quantify the environmental and socioeconomic impacts of these land use changes, focusing primarily on outcomes like greenhouse gas emissions and local soil and water contamination. Here, we provide the first estimates of how land use change impacts socioeconomic well-being through spatially dispersed disruptions to the atmospheric transport of terrestrial moisture. We identify who is most vulnerable to economic disturbance from changes to existing terrestrial moisture transport linkages and quantitatively assess the extent of potential harm.

Our analysis establishes that the socioeconomic importance of terrestrial moisture recycling is substantial, particularly in regions of low economic development. A disproportionate share of the global population resides outside predominantly inland, high-TMR-dependence regions – reflecting the tendency for major cities to develop along coastlines due to historical advantages[46] *and* where proximity to the ocean generates more abundant, ocean-sourced rainfall. Accordingly, we find that populated regions with the highest dependence on TMR are largely inland and coincide with the lowest-developed global areas – including northern South America and Central Africa. These areas currently face the highest exposure and vulnerability to disruption of existing terrestrial moisture flows.

Across the globe, we quantify that rainfed-dependent regions with low-income populations – where people are most dependent on agricultural output and face the highest adaptation constraints – receive an average of 10% of their annual rainfall from lands that are at high risk of deforestation. In these regions, we estimate that the economic costs of TMR disruption from deforestation threaten to suppress aggregate economic growth and potentially even reverse recent gains in agricultural productivity altogether. In contrast, much of the global north is fully insulated from such TMR-based risk, due both to lower dependence on terrestrial moisture recycling and due to lower vulnerability to rainfall shortages.

Overall, our analyses identify scope for adaptation opportunities from intentional land use changes – such as expanding irrigation and forestation efforts – echoing recent work promoting targeted rainfall enhancement as a co-benefit of reforestation efforts[14,16,17,47]. A growing literature – both using quasi-experimental[11,13,48] and field methods[49] – finds positive impacts of tree shelterbelts on crop production by offering wind breaks and improving the microclimate for growing conditions. Our simulated impacts of ET disruption suggest that forest loss in key deforestation hotspots would substantially reduce agricultural productivity in many downwind regions, leading to significant yield losses. These findings imply that TMR contributed by forests play a critical role in sustaining food production in many populated regions. Our analyses also uncover strong moisture linkages between croplands that point to untapped potential for sustainable management. Proactive policies that

promote adaptation strategies – such as the strategic siting of irrigation expansion, protection of key upwind source areas, and establishment of tree shelterbelts – may be key to the long-term resilience of food production and regional rainfall.

These results highlight the transboundary consequences of deforestation-driven moisture recycling losses and point toward the need for coordinated land use and conservation strategies. In particular, the finding that forests contribute substantially to downwind agricultural productivity suggests that forest conservation can serve as a climate-resilience and food security policy, especially in regions reliant on rainfed agriculture. These insights lend empirical support to global initiatives such as the 30x30 conservation target – which aims to protect 30% of Earth's land and water by 2030 – not only for biodiversity and carbon sequestration, but also for its indirect effects on human production through atmospheric moisture flows. Integrating moisture recycling considerations into spatial conservation planning can improve the cost-effectiveness of both domestic and international land use policy instruments.

Our analysis has important limitations. The Lagrangian moisture tracking model we rely on (available at https://doi.org/10.1594/PANGAEA.912710) should be interpreted as an approximation of the complex physical processes governing atmospheric moisture flows. Fully resolving these processes would require detailed representation of coupled water–energy balances and their interactions with biological and atmospheric dynamics across biomes and regions, which remains challenging given the scarcity of suitable observational data for model calibration. As a result, our analysis inherits uncertainties from these approximations, and this should be considered when interpreting the results.

Our global assessment of socioeconomic risk from disruptions to TMR relies on several simplifying assumptions. First, we assume homogeneous ET rates across land use categories within each grid cell, due to a lack of spatially resolved, land use-specific moisture flow data. Similarly, when simulating forest loss in deforestation hotspot regions, we impose a uniform proportional reduction in ET of 50% to approximate the effects of replacing forest with counterfactual land use types such as pasture or grassland. This ET reduction was chosen to reflect the consensus across a large body of empirical studies (see Economic valuation), but by construction this approximation abstracts from more complex post-deforestation vegetation dynamics. This assumption implicitly embeds a linear relationship between deforestation, ET, and precipitation in which reductions in cell-to-cell flows are additive and non-interacting. Some prior work has uncovered discontinuities in the deforestation-ET-precipitation relationship using mesoscale models where low rates of forest loss can actually *increase* rainfall[50]. While such nonlinearities are possible, we focus on emerging deforestation hotspots, where current forest levels are beyond such critical thresholds, such that rainfall declines are expected to occur under deforestation[51].

Second, our analysis focuses on long-run average rates of moisture exchange between global land

areas and does not incorporate possible impacts of land use or land use change on extreme precipitation events in downwind localities. To our knowledge, no such estimates currently exist at global scale, although existing work suggests such extreme events play an outsized role in economic outcomes[40]. Third, we focus here on moisture exchange. Thus, when simulating deforestation impacts, we do not assess the additional local warming effects caused by deforestation, such as increased sensible heat fluxes and land-atmosphere feedbacks[52,53]. Future work could build on our analysis to investigate the joint effects of changing moisture and temperature under alternative land use scenarios.

Finally, we decompose terrestrial ET into three aggregate land use categories that include forests, rainfed croplands, irrigated croplands, and the remaining land cover types (including grasslands, wetlands, and inland water bodies). Forests are the dominant source of TMR globally, but other land uses such as grasslands also play a significant role in sustaining atmospheric moisture flows[6]. Our analysis of TMR disruption from land use change is focused on forests owing to their large contribution to global TMR flows, the fact that they are exposed to heightened risk of land use change (mostly deforestation to cropland and grazing land)[54], and the substantial expected shifts in evaporative flows that are likely to result from such changes, given forests' greater leaf area, deeper rooting, and perennial nature[55–57]. Extensions to our analysis that assess the impacts of other land use conversions on TMR disruption could help paint an increasingly comprehensive picture of the global economic value of stable terrestrial moisture flows.

Methods

Data

Global atmospheric moisture flows (UTrack) Global terrestrial-based atmospheric moisture flows, on a 1.0 degree resolution ($N = 17,674$) for both the source locations and downwind precipitation locations, were obtained from the UTrack dataset[20]. Tracked atmospheric moisture flows over 2008-2017 were aggregated into a matrix of bilateral connections between sources and sinks using ERA5 reanalysis data at the monthly level. The dataset was generated using "UTrack", a Lagrangian atmospheric moisture tracking model developed by[21] and forced with ERA5 atmospheric reanalysis data[58]. The model tracks moisture parcels from their point of evaporation through the atmosphere along trajectories calculated using local wind fields derived from the forcing data. At each time step, the moisture content of each parcel is apportioned to rainfall at its current location, based on ERA5 precipitation and precipitable water. Each moisture parcel is tracked for up to 30 days or until 99% of its water has been allocated to rainfall. The UTrack model was refined with detailed sensitivity analysis to test various assumptions and uncertainties affecting the accuracy of moisture tracking and hydrologically relevant statistics. Values exceeding 100% where the water balance is not closed (i.e., the tracked moisture accumulation exceeds observed reanalysis data) are winsorized to 100%. These occurrences happen in less than 6% of all cells and largely in the major

deserts of the world such as the Gobi or Sahara. The dataset is available from the PANGAEA archive at https://doi.pangaea.de/10.1594/PANGAEA.912710.

Weather data Data on ambient temperature and precipitation for the period 2003 to 2022 were collected from the ERA5 Reanalysis product provided by the Copernicus Climate Change Service Climate Data Store. The reanalysis covers the period from 1940 to today and combines model as well as observational data to construct a consistent dataset with global coverage on a large number of land and oceanic climate variables. Specifically, we obtained total precipitation at an hourly resolution and at a 0.25°-by-0.25° grid. We aggregate this data to the UTrack grid described above using area weighting and then calculate monthly average temperature in °C and monthly total precipitation in cm. The raw data can be obtained here: https://cds.climate.copernicus.eu/cdsapp#!/dataset/reanalysis-era5-single-levels?tab=overview.

Agricultural data Harvested area under rainfed and irrigated conditions were collected from the United Nations Food and Agriculture Organization's Global Agro-Ecological Zones (GAEZ v4) dataset. The dataset is a hybrid product based on census and modeled data, offering gridded crop information at a high spatial resolution of 5 arc-minutes for 26 different crops. Harvested area is based on aggregate national statistics from FAO statistics for the years 2009-2011 and downscaled to the individual spatial units. The GAEZ data can be sourced from https://gaez.fao.org.

Forest cover data Forest cover and forest loss data are derived from global maps of 21^{th}-century forest cover change generated from Landsat imagery (∼30 m resolution at the equator) by ref.[59]. The dataset provides annual observations of forest loss and cumulative forest gain from 2000 onward. We aggregated these data to a 0.5°× 0.5° spatial grid by summing the area of forest extent, loss, and gain within each cell. We then estimated net forest cover for each grid cell by updating the year-2000 baseline forest extent with annual loss and gain up to 2017, the year corresponding to the final year in the calibration period of the UTrack atmospheric flow data. The resulting 2017 map represents the share of each 0.5° grid cell covered by forest.

Population data We acquire global population distribution data from the Global Human Settlements Layer (GHSL) database, developed by the European Commission. This dataset encompasses estimates of residential population derived from census and administrative units and further disaggregated to the grid cell level. The data are available at 5-year intervals, spanning the years 1975 to 2020. For our analysis, we use data on the distribution of residential population for the year 2020, aggregated to the 1.0 degree grid resolution. Population data from the GHSL can be retrieved from: https://human-settlement.emergency.copernicus.eu/dataToolsOverview.php.

Income data We aggregate 2015 global Gross Domestic Product (GDP) and GDP per capita data from the 5 arc-min resolution provided by ref.[29] to the 1 degree grid resolution of UTrack. The

dataset is mostly based on sub-national income data compiled by ref.[60] and covers 82 countries, representing 85% of the global population and 92% of global total GDP (PPP) in 2015.

Measuring moisture sinks: terrestrial precipitation share

Defining the terrestrial precipitation share Using the grid cell-to-grid cell bilateral dataset of atmospheric moisture flows, we compute the volume of precipitation in grid cell i originating from terrestrial evaporation as:

$$P_i^T = \sum_{j=1}^{J} F_{ji}, \tag{1}$$

where F_{ji} denotes the volume of moisture (in liters) transported from source grid cell j to sink grid cell i. J includes all terrestrial grid cells while superscripts on P indicate source origin: terrestrial (T) or oceanic (O).

Total precipitation for location i, P_i, is then the sum of terrestrial- and ocean-sourced moisture flows:

$$P_i = P_i^T + P_i^O$$

and the terrestrial precipitation share (TPS) is calculated as:

$$TPS_i = \left(\frac{P_i^T}{P_i}\right) \times 100. \tag{2}$$

TPS_i is plotted for each terrestrial location globally in Fig. 2a. In grid cells where the moisture balance is not closed – i.e., $P_i^T > P_i$ due to tracking artifacts in the Utrack data[5] – we cap terrestrial precipitation at the total P_i derived from the ERA5 reanalysis dataset. These discrepancies are rare (found in only 6% of all grid cells) and typically observed in arid or sparsely populated regions (e.g., the Sahara, Saudi Arabian coastal regions, and the Gobi Desert), which contribute minimally to our vulnerability assessments.

Vulnerability-weighted distribution In Fig. 2b-d, we plot weighted terrestrial precipitation share distributions (TSP_i^w), and in some cases the distributions shown are conditional on another vulnerability measure to show exposure based on multiple dimensions. These distributions of TPS_i^w are computed as:

$$TPS_i^w = TPS_i \times V_i \mid 1[i \in Y_d],$$

where $V \in \{1$, population count, rainfed cropland (hectares)$\}$ in each grid cell and Y_d denotes income decile for $d = 1, 2, ..., 10$ or, as in the case of the last panel of Fig. 2, a threshold for low-income regions, where annual average income is less than $4,465 as defined by the World Bank.

Measuring moisture sources: terrestrial precipitation exports

To analyze each grid cell from the converse perspective – as a *moisture source* rather than a sink – we calculate the total volume of moisture exported from source cell j to all terrestrial sink cells i:

$$ET_j = \sum_{i=1}^{I} F_{ji}, \tag{3}$$

where ET_j represents the total evapotranspiration from source grid cell j that contributes to terrestrial precipitation elsewhere and I includes all terrestrial grid cells.

This "contribution" metric ET_j is mapped in Fig. 3a. In Fig. S2b-c, we show a breakdown of this metric in which we weight F_{ji} by the share of: *(i)* rainfed cropland in source grid cell i; and *(ii)* rainfed cropland only in low-income locations (where income per capita of the local population is below US$4,465, the World Bank classification for lower middle-income countries) in source grid cell i. The former metric is motivated by the large impact that precipitation has on agricultural output and incomes in low-income rainfed agricultural food systems[45]. Fig. S2a plots the global spatial distribution of rainfed cropland and of areas designated as lower middle-income under the FY23-24 World Bank income classification.

Moisture flows by land use and exposure categories In Fig. 3b, we display the contribution of each land use type $u \in \{$forest, rainfed cropland, irrigated cropland, other$\}$ to terrestrial moisture flows supporting rainfed agriculture using a two-step weighting procedure. Because our land use data is at a higher resolution than our TMR data, we can compute for each source location, j, the proportion of ET generated destined for rainfed agriculture destinations using the share of all sink cells i devoted to rainfed agriculture (s_i^{rainfed}):

$$ET_{j\to\text{rainfed}} = \sum_i F_{ji}\, s_i^{\text{rainfed}}.$$

Implicitly, this approach assumes that tracked moisture, F_{ji}, falls evenly over all areas in i. This is a necessary assumption, as we cannot resolve within-grid cell rainfall distributions using UTrack[20]. Second, we compute the contribution of land use type u within source cell j by weighting the total moisture flow from j to rainfed cropland ($ET_{j\to\text{rainfed}}$) by the share of land area in j devoted to land use type u, denoted s_j^u, where $u \in \{$forest, rainfed cropland, irrigated cropland, other$\}$, as above.

Finally, to express land use contributions in relative terms, we normalize the total flow from land use type u to rainfed cropland by the total volume of terrestrial-sourced precipitation received by all rainfed cropland globally. Summing over all source and sink cells yields the share of global terrestrial-sourced precipitation received by rainfed cropland that is attributable to each land use type u:

$$ET_{u\to\text{rainfed}} = \frac{\sum_j \left(s_j^u \sum_i F_{ji}\, s_i^{\text{rainfed}} \right)}{\sum_j \sum_i F_{ji}\, s_i^{\text{rainfed}}}. \tag{4}$$

We repeat this calculation for overall terrestrial-sourced precipitation where s_i^{rainfed} is replaced by 1 (first bar in Fig. 3b), and for rainfed cropland only in low-income regions (third bar in Fig. 3b) where

$$s_i^{\text{rainfed}} = \begin{cases} s_i^{\text{rainfed}}, & \text{if } \text{GDP}_{pc,i} < 4465 \\ 0, & \text{otherwise} \end{cases}.$$

The results of this exercise are plotted in Fig. 3b.

Characterizing disruption to TMR flows from deforestation in emerging hotspots

Definition of emerging deforestation hotspots We focus our analysis on the disruption to TMR caused by deforestation in a set of emerging deforestation hotspots. To do so, we adopt the definition of a deforestation hotspot from ref.[31]: a deforestation hotspot is an area that exhibits statistically significant clustering in the spatial pattern of forest loss. To identify such hotspots, the authors conduct a spatial clustering of forest loss exercise in which they take into account the temporal signature of forest loss in each cluster. Specifically, they first identify spatial neighborhoods of statistically significant forest loss using the Queens Case Contiguity method. Second, they use the Mann-Kendall statistic[61] to test whether a statistically significant temporal trend exists through each grid cell's 14-year time series of the Getis-Ord Gi* statistic (a measure of the intensity of clustering of high values in a locality relative to its neighbor). Ref.[31] then assign each grid cell a deforestation category based on the cluster and its Getis-Ord Gi* statistic (e.g., intensifying to an increasing trend, persistent to a constant trend, and diminishing to a decreasing trend). Ref.[31] denote deforestation hotspots as all clusters that have a statistically significant increasing trend for all or some period of the period of analysis between 2000-2014.

To denote grid cells falling into emerging deforestation hotspots, we let j index source grid cells (i.e., where evapotranspiration originates), and i index sink grid cells (i.e., where precipitation falls), as previously defined. We then define source areas affected by deforestation as $d_j \in \{0, 1\}$, a binary

indicator equal to 1 if source cell j lies within a deforestation hotspot, and 0 otherwise.

Calculating deforestation-driven TMR disruption For each sink cell i, define the volume of its incoming moisture that originates from sources at risk of deforestation as:

$$P_i^{\text{risk}} = \sum_j \mathbb{1}(d)_j \cdot \mathrm{F}_{ji}$$

We then compute the following summary statistics for rainfed cropland:

$$TPS_i^{\text{risk}} = \frac{1}{N} \sum_i \frac{P_i^{\text{risk}}}{P_i} \times s_i^{\text{rainfed}}.$$

As in the previous section, we repeat this calculation for overall global "at-risk" precipitation share, where s_i^{rainfall} is replaced by 1, and for rainfed cropland only in low-income regions where

$$s_i^{\text{rainfed}} = \begin{cases} s_i^{\text{rainfed}}, & \text{if } \mathrm{GDP}_{pc,i} < 4465 \\ 0, & \text{otherwise} \end{cases}.$$

The results of this deforestation risk analysis for various measures of socioeconomic exposure are plotted in Fig. S3b.

Economic valuation

Estimating nonlinear impacts of precipitation on global economic activity The physically-based metrics detailed above offer a limited perspective on socioeconomic vulnerability, as they are unable to monetize the implications of TMR disruption in terms of damages to productive output. In particular, analysis based on physical units (e.g., terrestrial precipitation share) implicitly treats every unit of moisture as equally valuable, while economic theory and evidence indicate that, like other inputs to production, precipitation has declining marginal value to economic output.

To translate the human impacts of TMR disruption into economically meaningful terms, we build on a foundation of empirically estimated production functions that relate the quantities of precipitation in a given location and year to growth in (1) aggregate gross domestic product per capita (GDP) output and in the (2) productivity of the agricultural sector. These production functions typically take a quadratic form to capture the diminishing returns of increasing precipitation. To accurately capture the range of potential economic impacts at the continent level, we systematically replicated, resampled data, and re-estimated the key relationship using the original data and model specifications from refs.[41], [40], and [42] using a block bootstrap, blocking by region (for economic

growth) and country (for agricultural TFP). This bootstrapped approach allows us to first generate a range of estimated effects related to the simulated cell-level changes in TMR-driven precipitation, which are then aggregated over each continent to yield distributions of net effect that reflect sampling uncertainty. We use this approach to estimate a plausible range of aggregate economic losses driven by precipitation reduction due to forest loss in deforestation hotspots globally.

To reflect uncertainty in model and data sources, we draw on the empirical strategies of two recent, replicable studies estimating the impact of precipitation on GDP growth rates: Damania et al. [41] and Kotz et al. [40]. For agricultural productivity, we rely on data and methods from Ortiz-Bobea et al. [42], which is the only study to estimate the empirical relationship between precipitation and agricultural total factor productivity (TFP) on a global scale. Table M1 provides a comparison highlighting the main differences in data sources, outcome of interest, and parameter estimates among the three studies. Kotz et al. [40] estimates the quadratic relationship between annual precipitation and GDP growth rates over 1979-2019 using new subnational economic data [62] compiled from various governmental or administrative agencies, while Damania et al. [41] estimates this relationship over 1990-2014 using grid-cell level GDP per capita data [29] downscaled from a different source of subnational economic data [63]. The geographical coverage is 77 and 82 countries, respectively.

Our agricultural productivity framework comes from Ortiz-Bobea et al. [42], who estimate the relationship between "green-season" precipitation and agricultural TFP at the country level using a set of TFP indices obtained from the US Department of Agriculture's Economic Research Service for 172 countries over 1961-2015. Agricultural TFP is a measure that incorporates aggregate production value of the agricultural sector, accounting for input responses such as in land, labor, and chemicals; and thus captures interactions between output and input adjustments. Ortiz-Bobea et al. [42] focuses on green-season precipitation only, which is the 5-month period centered around the greenest month of the year of each country. Our month-level dataset of cell-to-cell TMR flows allows us to utilize this framework because we are able to calculate "green-season" precipitation changes by aggregating precipitation losses only occurring in green-season months under our deforestation scenario.

In all papers, the general relationship that equates economic or agricultural TFP growth to precipitation in location i in year t is

$$\text{Growth}_{it} = \beta_1 P_{it} + \beta_2 P_{it}^2 + \boldsymbol{\gamma}^\top \mathbf{Z}_{it} + \mu_i + \lambda_t + f_c(t) + \varepsilon_{it}, \tag{5}$$

where P denotes precipitation, $\mathbf{Z}$ is a vector of other climate controls such as quadratic functions of temperature as in [41,42] or other moments of the rainfall or temperature distributions as in [40]. Growth is computed as the year-to-year difference in the natural logarithm of GDP or TFP measure. Fixed effects at the location (μ) and year (λ) levels capture location- and time-specific baseline growth

rates. Because the model is specified in growth terms, the inclusion of a unit-specific dummy variable μ_i is analogous to controlling for a linear unit-specific time trend in levels of output. The specification in Damania et al. [41] also includes functions of country-level trends, denoted by $f_c(t)$, as controls. Our key parameters of interest β_1 and β_2 are the modeled quadratic parameters describing the relationship between aggregate growth and total precipitation.

Using equation (5), we compute the expression for the change in GDP or ag TFP growth in each location i resulting from simulated deforestation (loss of P_i^{risk}) in each grid cell:

$$\begin{aligned}
\Delta \text{ Growth}_i &= \beta_1 P_i' + \beta_2 P_i'^{\,2} + \boldsymbol{\gamma}^\top \mathbf{Z}_{it} + \mu_i + \lambda_t + f_c(t) + \varepsilon_{it} \\
&\quad - \left[\beta_1 P_i + \beta_2 P_i^2 + + \boldsymbol{\gamma}^\top \mathbf{Z}_{it} + \mu_i + \lambda_t + f_c(t) + \varepsilon_{it}\right] \\
&= \beta_1 (P_i' - P_i) + \beta_2 (P_i'^{\,2} - P_i^2) \\
&= -\beta_1 P_i^{\text{risk}} - 2\beta_2 P_i P_i^{\text{risk}} + \beta_2 (P_i^{\text{risk}})^2. \qquad (6)
\end{aligned}$$

Given that the fixed effects and other climate control variables that are assumed to be held constant (e.g., standardized monthly rainfall deviations) cancel out, our final expression for the change in growth in equation (6) is a function of observable and estimated quantities. We obtain P_i, mean annual rainfall from the ERA-5 reanalysis of historical observed precipitation, derive P_i^{risk} using our spatial model of cell-to-cell moisture flows, and reanalyze estimates of the rainfall-growth parameters, $\hat{\beta}_1$ and $\hat{\beta}_2$ using the established framework described earlier. For both studies on aggregate GDP [40,41], the parameters β_1 and β_2 differ across space, as lower-income (developing) countries are found to be far more sensitive to rainfall variations than are higher-income nations, presumably due to differences in capital investments (e.g., drilling groundwater wells, investing in dams) and other forms of adaptation. Fig. M1 illustrates the method used to conduct this calculation.

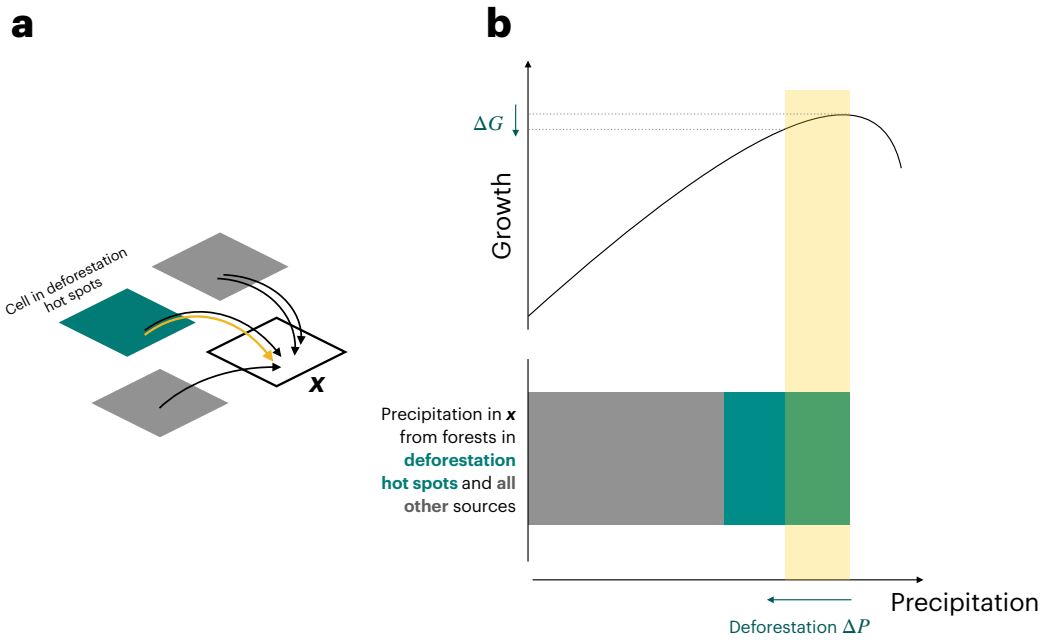


Figure M1: Illustrating the economic valuation methodology used to quantify the costs of deforestation on downwind precipitation and measures of economic growth. Panel **a** illustrates the determination of the amount of downwind precipitation change to cell X when one of its upwind cells is in a deforestation hotspot (green). The yellow arrow illustrates the modeled 50% reduction in atmospheric moisture flows from deforestation hotspots, representing half of the moisture originally contributed by these areas. Panel **b** shows how we translate the net change in precipitation for each cell globally into an impact on growth in aggregate Gross Domestic Product (GDP) and agricultural total factor productivity using established precipitation-growth response functions from Kotz et al.[40], Damania et al.[41], Ortiz-Bobea et al.[42].

Study	Sample	$\beta_1(\times 10^{-5})$	$\beta_2(\times 10^{-9})$	Data Source	Spatial Resolution	Years
Kotz et al. (2022)	Developing	3.684 (0.957)	−2.653 (1.317)	Database of Subnational Economic (DoSE)[62], ERA-5 climate data	Admin-1-level	1979–2019
	High-income	−2.590 (0.830)	2.403 (1.590)			
Damania et al. (2020)	Developing	1.94 (0.381)	−3.0 (0.081)	Downscaled GDPPC grid-level data (0.5°)[29], UDEL v3.01 climate data	0.5° grid-cell-level	1990–2014
	High-income	−0.264 (0.494)	−0.87 (1.18)			
Ortiz-Bobea et al. (2021)	All	18.2 (3.50)	−182 (0.410)	USDA ERS TFP data, FAOSTAT, GMFD climate data	Country-level	1961–2015

Table M1: Empirical estimates of annual cumulative precipitation impacts on growth in aggregate Gross Domestic Product and agricultural productivity. Coefficients are reported for the linear and quadratic terms of annual precipitation in Damania et al.[41], Kotz et al.[40], and Ortiz-Bobea et al.[42]. Values in parentheses report standard errors. Estimates are separated by sample (developing vs. high-income) where applicable.

Estimating counterfactual TMR under forest loss in hotspot regions To account for the fact that alternative land use (e.g., grassland, pasture, or soybean agriculture) continues to provide some evapotranspiration (ET) even after forest loss, in our simulations we conservatively reduce ET in deforestation hotspot grid cells by 50%, rather than assuming complete elimination. This adjustment is informed by empirical evidence suggesting that ET reductions from deforestation are substantial but typically not total, due to residual vegetation and regrowth.

Previous studies estimate that deforestation can reduce regional precipitation by a wide range, depending on biome and scale: in the Congo Basin, losses of 10–20%[55] to 50%[64] have been reported, while in the Amazon, reductions range from 4-30%[8] to 55–70%[65]. Although these studies quantify the precipitation response to *observed* forest loss at various spatial scales, estimates derived from large-scale deforestation can be interpreted as approximate upper bounds on the reduction in ET. At such scales, most moisture that would have been recycled back into the region originates from the forest itself, so the observed decline in precipitation closely reflects the maximum amount of ET that deforestation could remove from the regional hydrological cycle.

The cell-level estimated changes in growth rates based on all studies are mapped in Figs. S4 and S5. In the main text, we present the aggregated growth rate changes and their respective 95% confidence intervals at the continent level (Fig. 4). As described, we apply a bootstrap approach to propagate uncertainty from empirical estimates from all three studies into our continent-level estimates of impacts.

Competing interests The authors have no competing interests.

Code availability The code to reproduce the analysis is available at: https://doi.org/10.5281/zenodo.18072726.

Data availability Global atmospheric moisture flows, ERA-5 climate data, land use (agricultural acreage and forest cover), population, and income date are publicly available at https://doi.pangaea.de/10.1594/PANGAEA.912710, https://cds.climate.copernicus.eu/cdsapp#!/dataset/reanalysis-era5-single-levels?tab=overview, https://gaez.fao.org, https://hub.arcgis.com/documents/85caa1aa8de2422894f6c1f11ae1d524/explore, https://human-settlement.emergency.copernicus.eu/dataToolsOverview.php, and https://datadryad.org/dataset/doi:10.5061/dryad.dk1j0, respectively. All processed data required for analysis and figure generation are available at: https://doi.org/10.5281/zenodo.18072726.

References

[1] Patrick W. Keys, Lan Wang-Erlandsson, Line J. Gordon, Victor Galaz, and Jonas Ebbesson. Approaching moisture recycling governance. *Global environmental change: human and policy dimensions*, 45:15–23, 2017. ISSN 0959-3780. doi: 10.1016/j.gloenvcha.2017.04.007. URL https://www.sciencedirect.com/science/article/pii/S0959378016306902.

[2] P. W. Keys, R. J. van der Ent, L. J. Gordon, H. Hoff, R. Nikoli, and H. H. G. Savenije. Analyzing precipitationsheds to understand the vulnerability of rainfall dependent regions. *Biogeosciences*, 9(2):733–746, 2012. ISSN 1726-4170. doi: 10.5194/bg-9-733-2012. URL https://bg.copernicus.org/articles/9/733/2012/bg-9-733-2012.pdf.

[3] Patrick W. Keys, Miina Porkka, Lan Wang-Erlandsson, Ingo Fetzer, Tom Gleeson, and Line J. Gordon. Invisible water security: Moisture recycling and water resilience. *Water Security*, 8:100046, December 2019. ISSN 2468-3124. doi: 10.1016/j.wasec.2019.100046. URL https://www.ncbi.nlm.nih.gov/pmc/articles/PMC6910651/.

[4] Rudi J. van der Ent, Hubert H. G. Savenije, Bettina Schaefli, and Susan C. Steele-Dunne. Origin and fate of atmospheric moisture over continents. *Water Resources Research*, 46(9), 2010. ISSN 1944-7973. doi: 10.1029/2010WR009127. URL https://onlinelibrary.wiley.com/doi/abs/10.1029/2010WR009127.

[5] Elena De Petrillo, Simon Felix Fahrländer, Marta Tuninetti, Lauren Seaby Andersen, Luca Monaco, Luca Ridolfi, and Francesco Laio. Reconciling tracked atmospheric water flows to close the global freshwater cycle. *Communications Earth & Environment*, 6:347, 5 2025. ISSN 2662-4435. doi: 10.1038/s43247-025-02289-y.

[6] Taikan Oki and Shinjiro Kanae. Global hydrological cycles and world water resources. *Science*, 313(5790):1068–1072, 2006.

[7] Sofie A. te Wierik, Erik L. H. Cammeraat, Joyeeta Gupta, and Yael A. Artzy-Randrup. Reviewing the impact of land use and land-use change on moisture recycling and precipitation patterns. *Water resources research*, 57(7), 2021. ISSN 0043-1397. doi: 10.1029/2020wr029234. URL http://dx.doi.org/10.1029/2020wr029234.

[8] DV Spracklen and LJGRL Garcia-Carreras. The impact of amazonian deforestation on amazon basin rainfall. *Geophysical Research Letters*, 42(21):9546–9552, 2015.

[9] Simon Felix Fahrländer, Lan Wang-Erlandsson, Agnes Pranindita, and Fernando Jaramillo. Hydroclimatic vulnerability of wetlands to upwind land use changes. *Earth's Future*, 12, 3 2024. ISSN 2328-4277. doi: 10.1029/2023EF003837. URL https://agupubs.onlinelibrary.wiley.com/doi/10.1029/2023EF003837.

[10] Rafael Araujo. The value of tropical forests to hydropower. *Energy economics*, 129(107205): 107205, 2024. ISSN 0140-9883. doi: 10.1016/j.eneco.2023.107205. URL https://www.sciencedirect.com/science/article/pii/S014098832300703X.

[11] Tianshu Li. Protecting the breadbasket with trees? the effect of the great plains shelterbelt project on agriculture. *Land economics*, 97(2):321–344, 2021. ISSN 0023-7639. doi: 10.3368/le.97.2.321. URL http://le.uwpress.org/content/97/2/321.abstract.

[12] Justin E Bagley, Ankur R Desai, Keith J Harding, Peter K Snyder, and Jonathan A Foley. Drought and deforestation: has land cover change influenced recent precipitation extremes in the amazon? *Journal of Climate*, 27(1):345–361, 2014.

[13] Florian Grosset, Anna Papp, and Charles Taylor. Rain follows the forest: Land use policy, climate change, and adaptation. *SSRN Electronic Journal*, 2023. ISSN 1556-5068. doi: 10.2139/ssrn.4333147. URL https://papers.ssrn.com/abstract=4333147.

[14] Agnes Pranindita, Adriaan J. Teuling, Ingo Fetzer, and Lan Wang-Erlandsson. Forests support global crop supply through atmospheric moisture transport. *Nature water*, 3(11):1243–1255,

2025. ISSN 2731-6084. doi: 10.1038/s44221-025-00518-4. URL https://www.nature.com/articles/s44221-025-00518-4.

[15] Johan Rockstrom, Mariana Mazzucato, Lauren Seaby Andersen, Simon Felix Fahrlander, and Dieter Gerten. Why we need a new economics of water as a common good. *Nature*, 615: 794–797, March 2023. doi: 10.1038/d41586-023-00800-z.

[16] Maganizo Kruger Nyasulu, Ingo Fetzer, Lan Wang-Erlandsson, Fabian Stenzel, Dieter Gerten, Johan Rockström, and Malin Falkenmark. African rainforest moisture contribution to continental agricultural water consumption. *Agricultural and forest meteorology*, 346(109867): 109867, 2024. ISSN 0168-1923. doi: 10.1016/j.agrformet.2023.109867. URL https://www.sciencedirect.com/science/article/pii/S0168192323005579.

[17] Arie Staal, Jolanda J. E. Theeuwen, Lan Wang-Erlandsson, Nico Wunderling, and Stefan C. Dekker. Targeted rainfall enhancement as an objective of forestation. *Global change biology*, 30(1):e17096, 2024. ISSN 1354-1013. doi: 10.1111/gcb.17096. URL http://dx.doi.org/10.1111/gcb.17096.

[18] Justin E. Bagley, Ankur R. Desai, Paul A. Dirmeyer, and Jonathan A. Foley. Effects of land cover change on moisture availability and potential crop yield in the world's breadbaskets. *Environmental research letters*, 7(1):014009, 2012. ISSN 1748-9326. doi: 10.1088/1748-9326/7/1/014009. URL https://iopscience.iop.org/article/10.1088/1748-9326/7/1/014009/meta.

[19] A. Reisinger, M. Garschagen, K. J. Mach, M. Pathak, E. Poloczanska, M. van Aalst, A. C. Ruane, M. Hoden, M. Hurlber, K. Mintenbeck, R. Pedace, M. Rojas Corradi, D. Viner, C. Vera, S. Kreibiehl, B O'Neill, H.-O. Pörtner, J. Sillmann, R. Jones, and R. Ranasinghe. The concept of risk in the ipcc sixth assessment report: A summary of cross-working group discussions: Guidance for ipcc authors, 2020.

[20] Obbe A. Tuinenburg, Jolanda J. E. Theeuwen, and Arie Staal. High-resolution global atmospheric moisture connections from evaporation to precipitation. *Earth Syst. Sci. Data*, 12(4): 3177–3188, December 2020. ISSN 1866-3508. doi: 10.5194/essd-12-3177-2020.

[21] Obbe A. Tuinenburg and Arie Staal. Tracking the global flows of atmospheric moisture and associated uncertainties. *Hydrology and Earth System Sciences*, 24:2419–2435, 5 2020. ISSN 1607-7938. doi: 10.5194/hess-24-2419-2020. URL https://hess.copernicus.org/articles/24/2419/2020/. - explanation of lagrangian and eulerian moisture tracking models - assessment of uncertainties in the model computation using ERA5 and a new set of moisture tracking models - best results: Lagrangian models but considerable uncertainty regarding turbulent mixing remains - UTtrack-atmosheric-moisture.

[22] Barbara JB Stunder. An assessment of the quality of forecast trajectories. *Journal of Applied Meteorology and Climatology*, 35(8):1319–1331, 1996.

[23] Arie Staal, Pim Meijer, Maganizo Kruger Nyasulu, Obbe A. Tuinenburg, and Stefan C. Dekker. Global terrestrial moisture recycling in shared socioeconomic pathways. *Earth System Dynamics*, 16:215–238, 1 2025. ISSN 2190-4987. doi: 10.5194/esd-16-215-2025.

[24] Nico Wunderling, Frederik Wolf, Obbe A. Tuinenburg, and Arie Staal. Network motifs shape distinct functioning of earth's moisture recycling hubs. *Nature Communications*, 13(1):1–8, November 2022. doi: 10.1038/s41467-022-34229-1.

[25] Obbe A. Tuinenburg, Joyce H. C. Bosmans, and Arie Staal. The global potential of forest restoration for drought mitigation. *Environmental research letters*, 17(3):034045, 2022. ISSN 1748-9326. doi: 10.1088/1748-9326/ac55b8. URL https://iopscience.iop.org/article/10.1088/1748-9326/ac55b8/meta.

[26] Bernardo M. Flores, Encarni Montoya, Boris Sakschewski, Nathália Nascimento, Arie Staal, Richard A. Betts, Carolina Levis, David M. Lapola, Adriane Esquível-Muelbert, Catarina

Jakovac, Carlos A. Nobre, Rafael S. Oliveira, Laura S. Borma, Da Nian, Niklas Boers, Susanna B. Hecht, Hans Ter Steege, Julia Arieira, Isabella L. Lucas, Erika Berenguer, José A. Marengo, Luciana V. Gatti, Caio R. C. Mattos, and Marina Hirota. Critical transitions in the amazon forest system. *Nature*, 626(7999):555–564, 2024. ISSN 0028-0836. doi: 10.1038/s41586-023-06970-0. URL https://www.nature.com/articles/s41586-023-06970-0.

[27] John Worden, David Noone, Kevin Bowman, Tropospheric Emission Spectrometer Science Team, and Data contributors. Importance of rain evaporation and continental convection in the tropical water cycle. *Nature*, 445(7127):528–532, 2007. ISSN 0028-0836. doi: 10.1038/nature05508. URL https://www.nature.com/articles/nature05508.

[28] Yan Jiang and Jennifer A. Burney. Crop water origins and hydroclimate vulnerability of global croplands. *Nature sustainability*, page 1–14, 2025. ISSN 2398-9629. doi: 10.1038/s41893-025-01662-1. URL https://www.nature.com/articles/s41893-025-01662-1.

[29] Matti Kummu, Maija Taka, and Joseph H. A. Guillaume. Gridded global datasets for Gross Domestic Product and Human Development Index over 1990–2015. *Sci. Data*, 5(180004):1–15, February 2018. ISSN 2052-4463. doi: 10.1038/sdata.2018.4.

[30] Arjen Y Hoekstra and Mesfin M Mekonnen. The water footprint of humanity. *Proceedings of the national academy of sciences*, 109(9):3232–3237, 2012.

[31] Nancy L Harris, Elizabeth Goldman, Christopher Gabris, Jon Nordling, Susan Minnemeyer, Stephen Ansari, Michael Lippmann, Lauren Bennett, Mansour Raad, Matthew Hansen, and Peter Potapov. Using spatial statistics to identify emerging hot spots of forest loss. *Environmental Research Letters*, 12(2):024012, Feb 2017. doi: https://doi.org/10.1088/1748-9326/aa5a2f. URL https://iopscience.iop.org/article/10.1088/1748-9326/aa5a2f.

[32] Luis Gimeno, Andreas Stohl, Ricardo M Trigo, Francina Dominguez, Kei Yoshimura, Lisan Yu, Anita Drumond, Ana María Durán-Quesada, and Raquel Nieto. Oceanic and terrestrial sources of continental precipitation. *Reviews of Geophysics*, 50(4), 2012.

[33] José Posada-Marín, Juan Salazar, Maria Cristina Rulli, Lan Wang-Erlandsson, and Fernando Jaramillo. Upwind moisture supply increases risk to water security. *Nature Water*, 2(9):875–888, 2024. ISSN 2731-6084. doi: 10.1038/s44221-024-00291-w. URL https://www.nature.com/articles/s44221-024-00291-w.

[34] Rogert Sorí, Raquel Nieto, Margarida L. R. Liberato, and Luis Gimeno. Oceanic versus terrestrial origin of El Niño Southern Oscillation–associated continental precipitation anomalies. *Ann. N.Y. Acad. Sci.*, 1504(1):202–214, November 2021. ISSN 0077-8923. doi: 10.1111/nyas.14665.

[35] Peter Potapov, Svetlana Turubanova, Matthew C. Hansen, Alexandra Tyukavina, Viviana Zalles, Ahmad Khan, Xiao-Peng Song, Amy Pickens, Quan Shen, and Jocelyn Cortez. Global maps of cropland extent and change show accelerated cropland expansion in the twenty-first century. *Nature food*, 3(1):19–28, 2022. ISSN 2662-1355. doi: 10.1038/s43016-021-00429-z. URL https://www.nature.com/articles/s43016-021-00429-z.

[36] Hannah Ritchie. Deforestation and forest loss. *Our World in Data*, 2021. https://ourworldindata.org/deforestation.

[37] Mostafa Javadian, Ali Behrangi, William Kolby Smith, and Joshua B. Fisher. Global trends in evapotranspiration dominated by increases across large cropland regions. *Remote sensing*, 12(7):1221, 2020. ISSN 2072-4292. doi: 10.3390/rs12071221. URL https://www.mdpi.com/2072-4292/12/7/1221.

[38] Malin Falkenmark and Johan Rockström. *Balancing water for humans and nature: the new approach in ecohydrology*. Earthscan, 2004.

[39] Lan Wang-Erlandsson, Arne Tobian, Ruud J. van der Ent, Ingo Fetzer, Sofie te Wierik, Miina Porkka, Arie Staal, Fernando Jaramillo, Heindriken Dahlmann, Chandrakant Singh, Peter

Greve, Dieter Gerten, Patrick W. Keys, Tom Gleeson, Sarah E. Cornell, Will Steffen, Xuemei Bai, and Johan Rockström. A planetary boundary for green water. *Nature reviews. Earth & environment*, 3(6):380–392, 2022. ISSN 2662-138X. doi: 10.1038/s43017-022-00287-8. URL https://www.nature.com/articles/s43017-022-00287-8.

[40] Maximilian Kotz, Anders Levermann, and Leonie Wenz. The effect of rainfall changes on economic production. *Nature*, 601(7892):223–227, January 2022. ISSN 1476-4687. doi: 10.1038/s41586-021-04283-8. URL https://www.nature.com/articles/s41586-021-04283-8. Publisher: Nature Publishing Group.

[41] R. Damania, S. Desbureaux, and E. Zaveri. Does rainfall matter for economic growth? Evidence from global sub-national data (1990–2014). *Journal of Environmental Economics and Management*, 102:102335, July 2020. ISSN 0095-0696. doi: 10.1016/j.jeem.2020.102335. URL https://www.sciencedirect.com/science/article/pii/S0095069620300589.

[42] Ariel Ortiz-Bobea, Toby R. Ault, Carlos M. Carrillo, Robert G. Chambers, and David B. Lobell. Anthropogenic climate change has slowed global agricultural productivity growth. *Nature Climate Change*, 11(4):306–312, Apr 2021. doi: https://doi.org/10.1038/s41558-021-01000-1. URL https://www.nature.com/articles/s41558-021-01000-1.

[43] Bradley Efron and Robert J Tibshirani. *An introduction to the bootstrap*. Chapman and Hall/CRC, 1994.

[44] Edward B Barbier and Jacob P Hochard. The impacts of climate change on the poor in disadvantaged regions. *Review of Environmental Economics and Policy*, 2018.

[45] Andrew Hultgren, Tamma Carleton, Michael Delgado, Diana R. Gergel, Michael Greenstone, Trevor Houser, Solomon Hsiang, Amir Jina, Robert E. Kopp, Steven B. Malevich, Kelly E. McCusker, Terin Mayer, Ishan Nath, James Rising, Ashwin Rode, and Jiacan Yuan. Impacts of climate change on global agriculture accounting for adaptation. *Nature*, 642(8068):644–652, 2025. ISSN 0028-0836. doi: 10.1038/s41586-025-09085-w. URL https://www.nature.com/articles/s41586-025-09085-w.

[46] Adam Smith. An inquiry into the nature and causes of the wealth of nations. *Readings in economic sociology*, pages 6–17, 2002.

[47] Arie Staal, Obbe A Tuinenburg, Joyce HC Bosmans, Milena Holmgren, Egbert H van Nes, Marten Scheffer, Delphine Clara Zemp, and Stefan C Dekker. Forest-rainfall cascades buffer against drought across the amazon. *Nature Climate Change*, 8(6):539–543, 2018.

[48] Yage Liu, Huidong Li, Fenghui Yuan, Lidu Shen, Minchao Wu, Wenliang Li, Anzhi Wang, Jiabing Wu, and Dexin Guan. Estimating the impact of shelterbelt structure on corn yield at a large scale using google earth and sentinel 2 data. *Environmental research letters*, 17(4):044060, 2022. ISSN 1748-9326. doi: 10.1088/1748-9326/ac58ab. URL https://iopscience.iop.org/article/10.1088/1748-9326/ac58ab/meta.

[49] T. E. Kowalchuk and E. de Jong. Shelterbelts and their effect on crop yield. *Canadian journal of soil science*, 75(4):543–550, 1995. ISSN 0008-4271. doi: 10.4141/cjss95-077. URL https://cdnsciencepub.com/doi/10.4141/cjss95-077.

[50] Cassiano D'Almeida, Charles J Vörösmarty, George C Hurtt, José A Marengo, S Lawrence Dingman, and Barry D Keim. The effects of deforestation on the hydrological cycle in amazonia: a review on scale and resolution. *International Journal of Climatology: A Journal of the Royal Meteorological Society*, 27(5):633–647, 2007.

[51] Argemiro Teixeira Leite-Filho, Britaldo Silveira Soares-Filho, Juliana Leroy Davis, Gabriel Medeiros Abrahão, and Jan Börner. Deforestation reduces rainfall and agricultural revenues in the brazilian amazon. *Nature communications*, 12(1):2591, 2021. ISSN 2041-1723. doi: 10.1038/s41467-021-22840-7. URL https://www.nature.com/articles/s41467-021-22840-7.

[52] Deborah Lawrence, Michael Coe, Wayne Walker, Louis Verchot, and Karen Vandecar. The unseen effects of deforestation: Biophysical effects on climate. *Frontiers in Forests and Global Change*, 5:756115, 2022. ISSN 2624-893X. doi: 10.3389/ffgc.2022.756115. URL https://www.frontiersin.org/journals/forests-and-global-change/articles/10.3389/ffgc.2022.756115/pdf.

[53] Edward W. Butt, Jessica C. A. Baker, Francisco G. Silva Bezerra, Celso von Randow, Ana P. D. Aguiar, and Dominick V. Spracklen. Amazon deforestation causes strong regional warming. *Proceedings of the National Academy of Sciences of the United States of America*, 120(45): e2309123120, 2023. ISSN 0027-8424. doi: 10.1073/pnas.2309123120. URL http://dx.doi.org/10.1073/pnas.2309123120.

[54] FAO. *The State of the World's Forests 2024: Forest-sector innovations towards a more sustainable future*. FAO, Rome, 2024. doi: 10.4060/cd1211en. URL https://doi.org/10.4060/cd1211en.

[55] C Smith, A Baker, and D V Spracklen. Tropical deforestation causes large reductions in observed precipitation. *Nature*, 615(7951):270–275, Mar 2023. doi: https://doi.org/10.1038/s41586-022-05690-1. URL https://www.nature.com/articles/s41586-022-05690-1#Sec5.

[56] David Ellison, Cindy E. Morris, Bruno Locatelli, Douglas Sheil, Jane Cohen, Daniel Murdiyarso, Victoria Gutierrez, Meine van Noordwijk, Irena F. Creed, Jan Pokorny, David Gaveau, Dominick V. Spracklen, Aida Bargués Tobella, Ulrik Ilstedt, Adriaan J. Teuling, Solomon Gebreyohannis Gebrehiwot, David C. Sands, Bart Muys, Bruno Verbist, Elaine Springgay, Yulia Sugandi, and Caroline A. Sullivan. Trees, forests and water: Cool insights for a hot world. *Global environmental change: human and policy dimensions*, 43:51–61, 2017. ISSN 0959-3780. doi: 10.1016/j.gloenvcha.2017.01.002. URL https://www.sciencedirect.com/science/article/pii/S0959378017300134.

[57] Boris Sakschewski, Werner Von Bloh, Markus Drüke, Anna Amelia Sörensson, Romina Ruscica, Fanny Langerwisch, Maik Billing, Sarah Bereswill, Marina Hirota, Rafael Silva Oliveira, et al. Variable tree rooting strategies are key for modelling the distribution, productivity and evapotranspiration of tropical evergreen forests. *Biogeosciences*, 18(13):4091–4116, 2021.

[58] Hans Hersbach, Bill Bell, Paul Berrisford, Shoji Hirahara, András Horányi, Joaquín Muñoz-Sabater, Julien Nicolas, Carole Peubey, Raluca Radu, Dinand Schepers, et al. The era5 global reanalysis. *Quarterly journal of the royal meteorological society*, 146(730):1999–2049, 2020.

[59] M. C. Hansen, P. V. Potapov, R. Moore, M. Hancher, S. A. Turubanova, A. Tyukavina, D. Thau, S. V. Stehman, S. J. Goetz, T. R. Loveland, A. Kommareddy, A. Egorov, L. Chini, C. O. Justice, and J. R. G. Townshend. High-resolution global maps of 21st-century forest cover change. *Science (New York, N.Y.)*, 342(6160):850–853, 2013. ISSN 0036-8075. doi: 10.1126/science.1244693. URL https://www.science.org/doi/10.1126/science.1244693.

[60] Nicola Gennaioli, Rafael La Porta, Florencio Lopez-de Silanes, and Andrei Shleifer. Human capital and regional development. *The Quarterly journal of economics*, 128(1):105–164, 2013.

[61] Henry B. Mann. Nonparametric tests against trend. *Econometrica: journal of the Econometric Society*, 13(3):245, 1945. ISSN 0012-9682. doi: 10.2307/1907187. URL http://www.jstor.org/stable/1907187.

[62] Matthias Kalkuhl and Leonie Wenz. The impact of climate conditions on economic production. evidence from a global panel of regions. *Journal of environmental economics and management*, 103(102360):102360, 2020. ISSN 0095-0696. doi: 10.1016/j.jeem.2020.102360. URL https://www.sciencedirect.com/science/article/pii/S0095069620300838.

[63] N. Gennaioli, R. L. Porta, R. L. Porta, Florencio Lopez-de-Silanes, Florencio Lopez-de-Silanes, A. Shleifer, and A. Shleifer. Human capital and regional development. *The Quarterly Journal of Economics*, 128(1):105–164, 2013. ISSN 0033-5533. doi: 10.1093/QJE/QJS050. URL

https://EconPapers.repec.org/RePEc:oup:qjecon:v:128:y:2013:i:1:p:105-164.

[64] Confidence Duku and Lars Hein. The impact of deforestation on rainfall in africa: a data-driven assessment. *Environmental Research Letters*, 16(6):064044–064044, Apr 2021. doi: https://doi.org/10.1088/1748-9326/abfcfb. URL https://iopscience.iop.org/article/10.1088/1748-9326/abfcfb.

[65] Mara Baudena, Obbe A Tuinenburg, Pendula A Ferdinand, and Arie Staal. Effects of land-use change in the amazon on precipitation are likely underestimated. *Global Change Biology*, 27(21):5580–5587, Aug 2021. doi: https://doi.org/10.1111/gcb.15810. URL https://onlinelibrary.wiley.com/doi/full/10.1111/gcb.15810.